PNAS RESEARCH ARTICLE | IMMUNOLOGY AND INFLAMMATION OPEN ACCESS

# SARS-CoV-2 spike does not interact with the T cell receptor or directly activate T cells

Stephanie A. Gaglione[a,b], Tatiana J. Rosales[c,d], Laura Schmidt-Hong[b,e], Brian M. Baker[c,d,1], and Michael E. Birnbaum[b,e,f,1]

Affiliations are included on p. 5.

Edited by Kristin Hogquist, University of Minnesota Medical School Twin Cities, Minneapolis, MN; received April 2, 2024; accepted June 25, 2024

**Suggested edit: SARS-CoV-2infection can induce multisystem inflammatory syndrome in children, which resembles superantigen-induced toxic shock syndrome. Recent work has suggested that the SARS-CoV-2 spike (S) protein could act as a superantigen by binding T cell receptors (TCRs) and inducing broad antigen-independent T cell responses. Structure-based computational modeling identified potential TCR-binding sites near the S receptor-binding domain, in addition to a site with homology to known neurotoxins. We experimentally examined the mechanism underpinning this theory—the direct interaction between the TCR and S protein. Surface plasmon resonance of recombinantly expressed S protein and TCR revealed no detectable binding. Orthogonally, we pseudotyped lentiviruses with SARS-CoV-2 S in both wild-type and prefusion-stabilized forms, demonstrated their functionality in a cell line assay, and observed no transduction, activation, or stimulation of proliferation of $CD8^+$ T cells. We conclude that it is unlikely that the SARS-CoV-2 spike protein engages nonspecifically with TCRs or has superantigenic character.**

SARS-CoV-2 | superantigen | T cell receptor

## Significance

Early in the severe acute respiratory syndrome coronavirus 2 (SARS-CoV-2) pandemic, severe multisystem inflammatory responses were observed in children. Symptoms of this condition resembled superantigen poisoning, which results in indiscriminate T cell activation via antigen-independent binding of superantigens to T cell receptors (TCRs). Sequence similarities between the SARS-CoV-2 spike protein and a bacterial superantigen led to the hypothesis that the spike protein could act as a superantigen. Although supported by structural modeling, this hypothesis has not yet found direct experimental support. Here, we studied the potential interaction of the spike protein with TCRs. With orthogonal biochemical and biological methods, we did not detect a spike-TCR molecular interaction. We conclude that it is unlikely that the SARS-CoV-2 spike protein engages nonspecifically with TCRs or has superantigenic character.

The scope and severity of the COVID-19 pandemic prompted a global effort to understand the mechanisms of disease (1). Understanding the etiology of multisystem inflammatory syndrome in children (MIS-C) and long-term sequelae associated with COVID-19 are of particular importance. Recent observations noting similarities between MIS-C and toxic shock syndrome elicited by bacterial superantigens led to the hypothesis that the SARS-CoV-2 spike (S) glycoprotein could act as a superantigen by directly binding T cell receptors (TCRs) (2). Structure-based computational modeling suggested the existence of potential TCR-binding sites near the S receptor-binding domain and the cleavage site between subunits S1 and S2, with the latter epitope on S resembling staphylococcal enterotoxin B (SEB), a known superantigen. Other potential TCR binding sites were also identified, including a site with homology to known neurotoxins. Modeling and sequence analyses work reaffirmed the TCR binding hypothesis (3–5), and recent work exploring the link between MIS-C and SARS-CoV-2 infection in children theorized activation by a viral superantigen (6). Further commentary has even raised the possibility of a link between the proposed TCR interaction and severe acute hepatitis in children (7). The potential serious clinical consequences have led investigators to urge experimental investigations into potential superantigen-like behavior of SARS-CoV-2 S (4, 7).

Bacterial superantigens, including SEB, are small proteins that cross-link germline-encoded Vβ regions of TCRs with class II MHC proteins in an antigen-independent fashion, triggering nonspecific TCR signaling by bringing T cells and antigen-presenting cells in direct proximity (8). The large size of the S protein relative to the TCR and MHC protein and the existence of multiple TCR binding sites would suggest different mechanisms for a S protein-based superantigen. Some TCRs, notably γδ TCRs, bind intact, non-MHC proteins (9). In limited contexts, αβ TCRs can have a similar capability, such as αβ TCRs identified in mice deficient for class I and class II MHC proteins and the CD4/CD8 coreceptors demonstrate binding to the cell adhesion protein CD155 (10, 11). Other proteins, such as antibodies, have been developed to interact with TCRs in an antigen-independent way (12). To date, however, there has been no experimental evidence of interactions between coronavirus S proteins and TCRs or direct activation of T cells by SARS-CoV-2 S. On the contrary, experimental data recently demonstrated that, unlike SEB, SARS-CoV-2 S does not stimulate inflammatory cytokine production in Jurkat cells and peripheral blood $CD4^+$ T cells (13). Considering the serious clinical consequences that would be associated with S protein superantigen-like behavior, we sought to determine whether SARS-CoV-2 S detectably binds the TCR or broadly activates T cells.

Competing interest statement: M.E.B. is a founder and consultant of Kelonia Therapeutics and Abata Therapeutics. M.E.B. is an equity holder of Kelonia Therapeutics, Abata Therapeutics, and 3T Biosciences. The lentiviral targeting approach in this manuscript is the subject of US patent applications with M.E.B. and S.A.G. as coinventors.

This article is a PNAS Direct Submission.



[1]To whom correspondence may be addressed. Email: brian-baker@nd.edu or mbirnb@mit.edu.

This article contains supporting information online at https://www.pnas.org/lookup/suppl/doi:10.1073/pnas.2406615121/-/DCSupplemental.

Published July 23, 2024.

## Results

We first attempted to measure a direct molecular interaction between recombinantly expressed, soluble versions of the S protein and TCR. As has been noted, recombinant SARS-CoV-2 S is typically stabilized in a fashion that alters one of the predicted superantigen-like TCR binding sites (5). However, other predicted binding sites remain and are conserved between the S proteins of SARS-CoV-2 and SARS-CoV. Indeed, predictive modeling suggests strong TCR binding to both proteins, with the neurotoxin-like region between Thr299 and Tyr351 predicted to have the second-highest TCR affinity in SARS-CoV-2 S and the highest TCR affinity in SARS-CoV S. We thus attempted to measure the interaction between readily available recombinant SARS-CoV S and the TCR using surface plasmon resonance (SPR), a commonly used biophysical assay capable of detecting strong to weak molecular interactions. We recombinantly expressed the T4H2 TCR, a well-characterized HLA-A*02:01-restricted TCR that recognizes the $gp100_{209}$ shared tumor antigen (sequence ITDQVPFSV) and variants (14). T4H2 uses TRBV19 and thus has the same β chain germline variable sequence as the TCR used in computational modeling (2). The SPR assay revealed clear binding of T4H2 to the peptide/HLA-A*02:01 complex (Fig. 1 *A* and *B*), but no clear binding to SARS-CoV S (Fig. 1*C*), although the S protein was recognized by recombinant, soluble angiotensin-converting enzyme-2 (ACE-2) (Fig. 1*D*).

Since we could not validate the computational modeling with SPR, we sought to examine protein interactions in a more native context, addressing potential limitations with the preparation and analysis of recombinant protein and permitting analysis of SARS-CoV-2 S (Fig. 2 and *SI Appendix*, Fig. S1). We recently described a lentiviral pseudotyping-based assay that uses specific infection to detect interactions between proteins displayed on the virus surface (including SARS-CoV-2 S protein) and cell surface proteins including the TCR (15). We created viruses pseudotyped with SARS-CoV-2 S protein and the influenza virus M1 peptide GL9 (sequence GILGFVFTL) presented by HLA-A*02:01 to test their interactions with cell-expressed receptors. We also transduced TCR αβ- J76 Jurkat cells with the JM22 TCR. JM22 recognizes GL9/HLA-A*02:01 and, like the T4H2 TCR, also uses the putative S-binding TRBV19 (16). Notably, computational studies employed the JM22 TCR in suggesting TCR binding to S proteins (2). While GL9/HLA-A*02:01-displaying

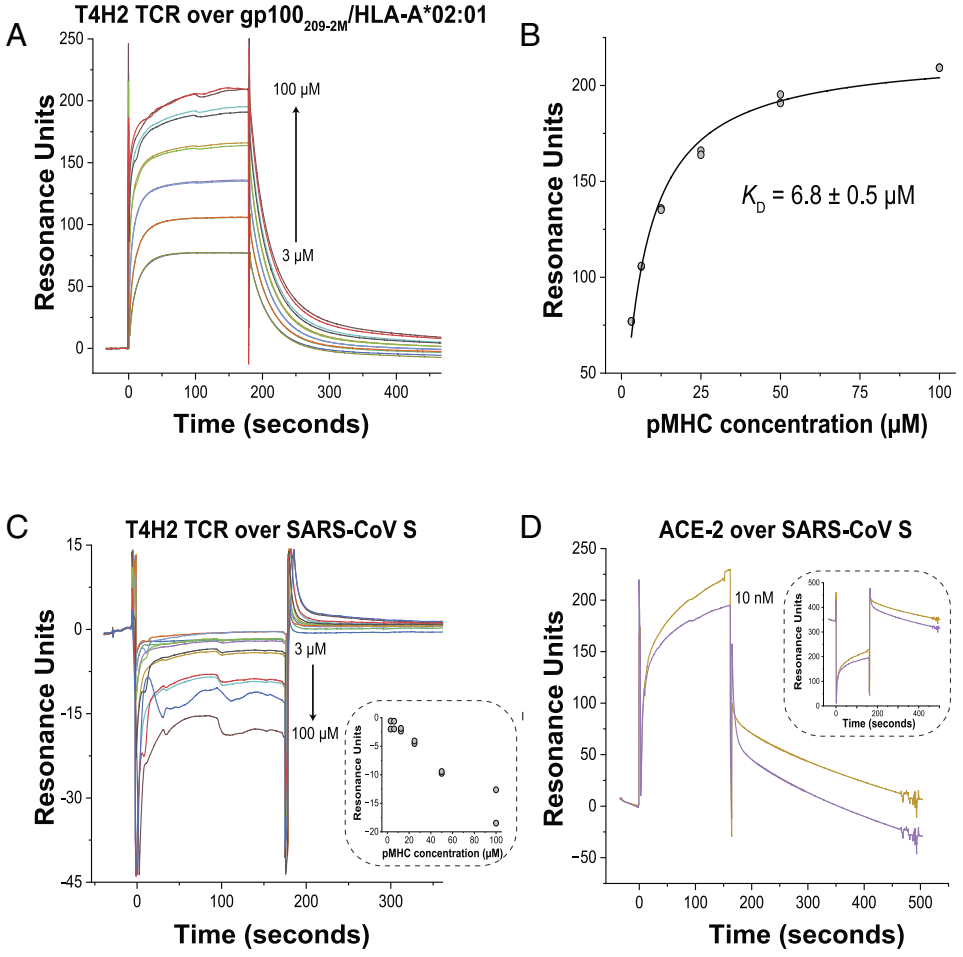


**Fig. 1.** Direct binding assays by SPR. (*A*) Reference-corrected SPR sensorgram for duplicate injections of increasing concentrations of the T4H2 TCR over a $gp100_{209\text{-}2M}$/HLA-A*02:01 surface. Positive responses after the start of the injections indicate binding. (*B*) Steady-state RU of the data in panel *A* vs. concentration of injected TCR (circles). The solid line is a fit to a single site binding isotherm, indicating a $K_D$ of 6.8 ± 0.5 μm. (*C*) As in panel *A* but increasing concentrations of TCR over a SARS-CoV S-surface. The lack of a positive response after injection indicates a lack of detectable binding. Small negative responses with increasing concentrations are attributable to the surface difference between the reference and experimental flowcell after coupling, resulting in more nonspecific binding to the reference, as commonly seen in SPR when specific binding is not evident. The *Inset* shows responses vs. concentration as in panel *B*. (*D*) As in panel *C*, but duplicate injections of 10 nM ACE-2 over S-coupled flowcell. The positive responses after the start of the injections indicate binding. Residual buffer mismatch between the ACE-2 sample and the SPR running buffer led to a bulk refractive index shift of 345 RU upon injection, corrected for in the pre- and postinjection signals. The uncorrected data are in the *Inset*, which still shows the binding of ACE-2 to the surface postinjection. For panels *A*, *C*, and *D*, off-scale injection start/stop spikes in the data were edited for clarity. Data shown are one of two replicates, each with the same overall outcome.

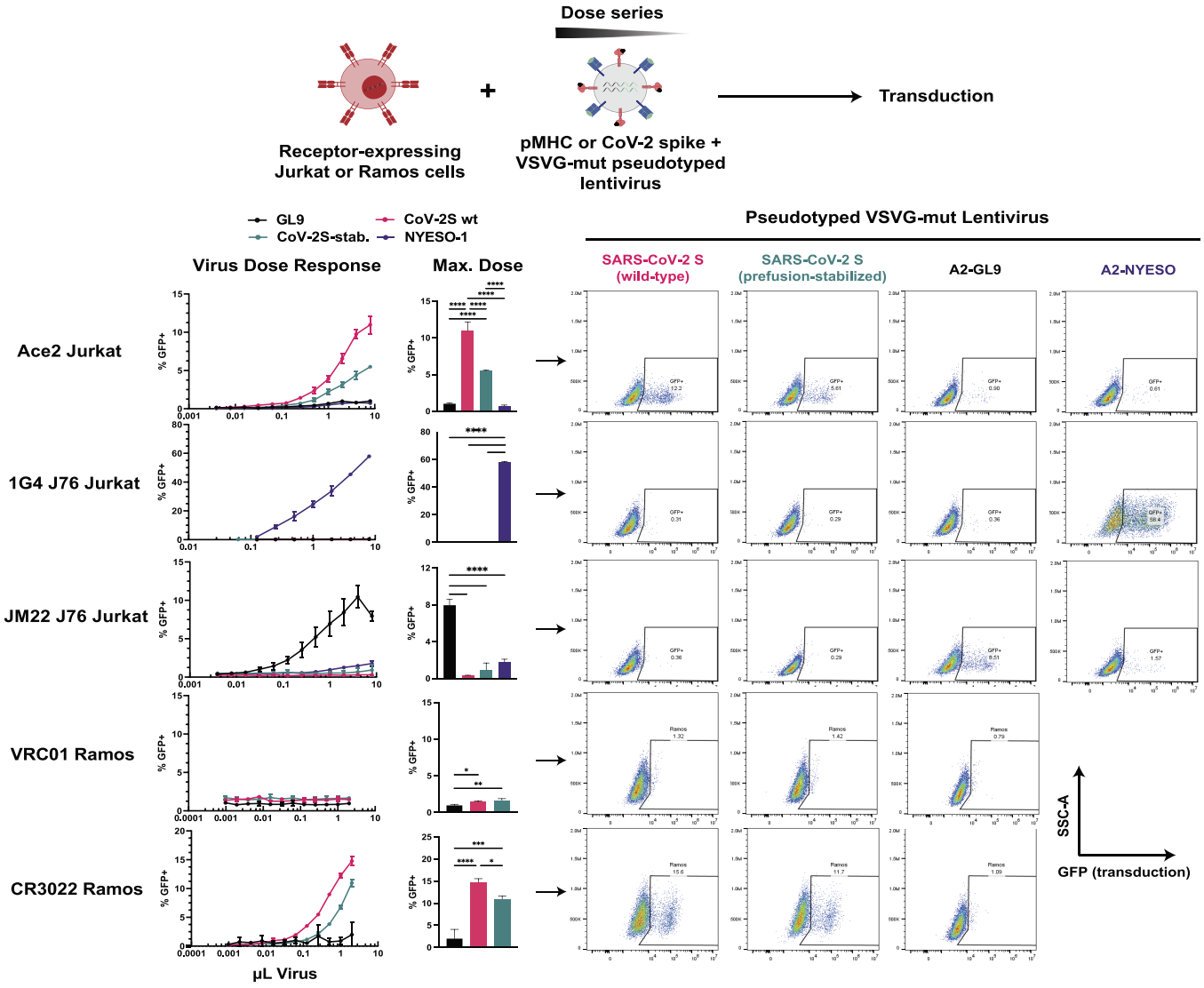


**Fig. 2.** SARS-CoV-2 displayed on lentivirus surface does not enable infection of T cells. Viruses pseudotyped with VSVG-mut and SARS-CoV-2 S (wild type and prefusion-stabilized) infect ACE2-expressing Jurkat and CR3022 BCR-expressing Ramos cells and do not infect TCR-expressing Jurkat J76 cells (JM22 and 1G4 TCRs) or off-target VRC01-expressing Ramos cells. Positive controls confirm the functionality of pseudotyped viruses and cell lines: GL9/HLA-A*02:01 virus for JM22 J76 cells and NYESO/HLA-A*02:01 virus for 1G4 J76 cells. Data shown as mean ± SD for $n = 3$ technical replicates in addition to representative flow cytometry plots. *P*-values calculated with a one-way ANOVA with Tukey's multiple comparisons correction. *$P < 0.05$; **$P < 0.01$; ***$P < 0.001$; and ****$P < 0.0001$.

viruses efficiently infected the JM22-expressing J76 cells, matching our previous data (15), no signal above baseline was noted when JM22-expressing J76 cells were exposed to viruses displaying SARS-CoV-2 S protein. The same SARS-CoV-2 S protein viruses were able to infect Jurkat cells expressing the ACE2 receptor as well as Ramos cells expressing a surface-bound version of the antibody CR3022, which is known to recognize SARS-CoV-2 S protein (17), demonstrating that the S protein was functionally displayed on the virus surface. Negative control Jurkat and Ramos lines did not show infection.

Finally, we examined SARS-CoV-2 S-mediated activation and proliferation of primary human T cells (Fig. 3). We mixed $CD8^+$ T cells from three donors with pseudotyped virus and assessed T cells for activation after 24 h and transduction and proliferation after 7 d. CD3/CD28 Dynabeads and viruses pseudotyped with an anti-CD3 Fab and the costimulatory receptor CD80 were used as positive controls. Cells exposed to CD3/CD28 DynaBeads or anti-CD3/CD80-pseudotyped virus displayed an increase in CD25 and CD69 expression within 24 h as well as strong proliferation. While anti-CD3/CD80-pseudotyped viruses transduced $CD8^+$ T cells, viruses pseudotyped with the prefusion-stabilized (18) or wild-type SARS-CoV-2 S did not activate, transduce, or stimulate proliferation of T cells, including cells expressing TCRs containing TRBV5-6, TRBV14, or TRBV13, three TCR V regions specifically hypothesized to interact with SARS-CoV-2 S (TRBV14 shown in Fig. 3 and *SI Appendix*, Fig. S1) (2).

## Discussion

Collectively, our results fail to show any direct interactions between TCRs and S proteins via orthogonal methods. We therefore conclude that it is unlikely that SARS-CoV-2 can operate as a broadly activating T cell superantigen and that this mechanism is unlikely to be the direct cause of MIS-C or pediatric severe acute hepatitis. Computational tools to predict protein structures and interactions are rapidly evolving and easily deployed, particularly with the introduction of AI methods (19, 20). However, accurate prediction of novel molecular interactions is still a particular challenge,

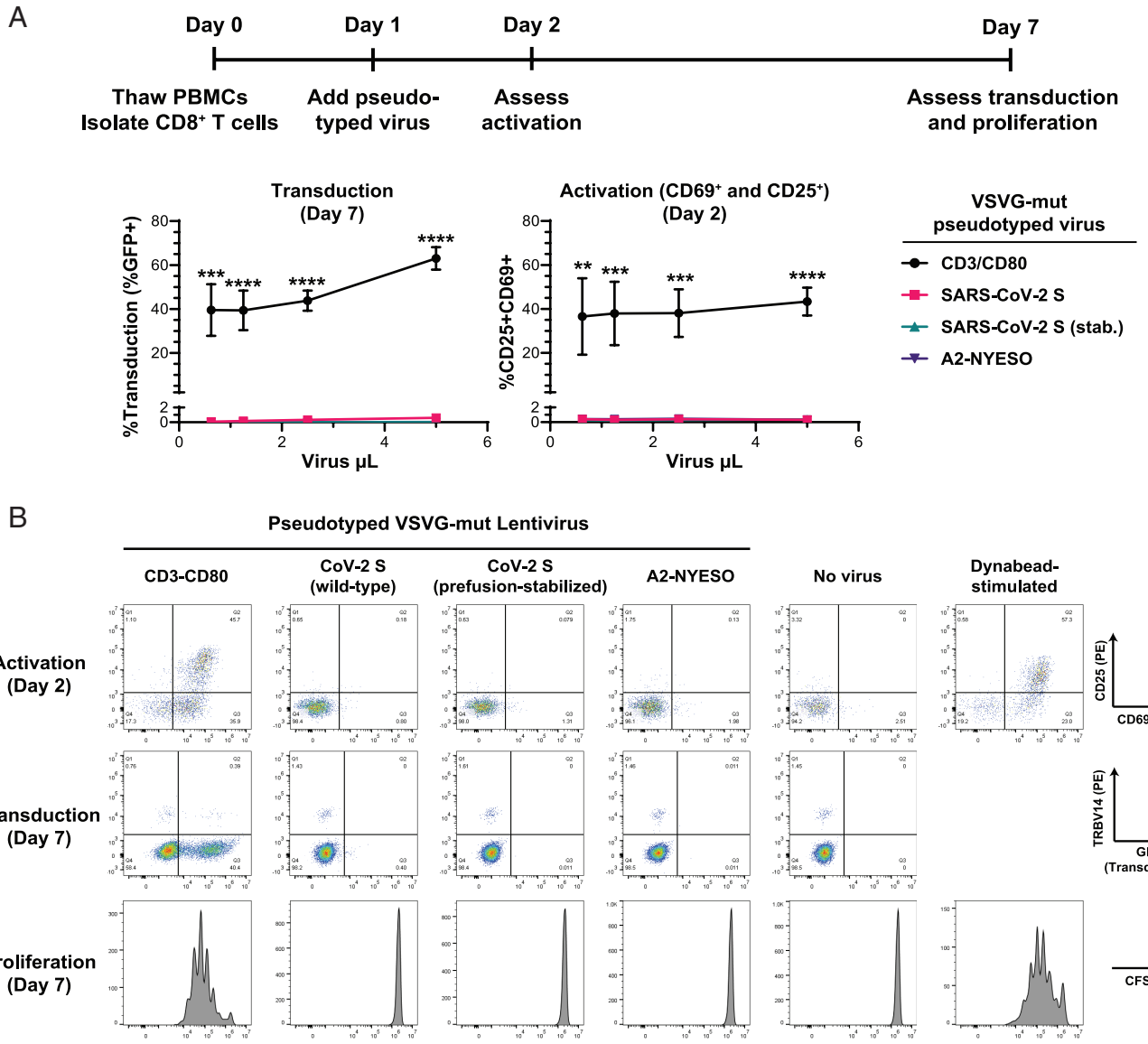


**Fig. 3.** SARS-CoV-2 displayed on lentivirus does not infect cells or induce T cell activation or proliferation. (*A*) Activation and infection of $CD8^+$ T cells by VSVG-mut pseudotyped viruses, measured as GFP expression on day 7 and CD69/CD25 expression on day 2 postisolation, respectively. Wild type and prefusion-stabilized SARS-CoV-2 S-pseudotyped virus do not transduce or activate $CD8^+$ T cells by pseudotyped viruses. CD3/CD80-VSVmut virus vs. all viruses: $^{****}P < 0.0001$, $^{***}P < 0.001$, $^{**}P < 0.01$; $P > 0.99$ (n.s.) for all pairwise comparisons of SARS-CoV-2 S, prefusion-stabilized SARS-CoV-2 S, and A2-NYESO viruses. *P* values determined by one-way ANOVA with Tukey's multiple comparisons correction. (*B*) SARS-CoV-2 S-pseudotyped viruses do not activate, transduce, or stimulate proliferation of $CD8^+$ T cells, inclusive of cells using TRBV14. Data shown as mean ± SD of $n = 3$ biological replicates, each consisting of $n = 3$ technical replicates, with representative flow plots.

including for TCRs (21–23), highlighting that experimental validation remains crucial for modeled data.

## Materials and Methods

**Media and Cells.** HEK293T (ATCC CRL-3216) were cultured in DMEM (ATCC) supplemented with 10% fetal bovine serum (FBS; Atlanta Biologics) and penicillin-streptomycin (Gibco). Jurkat (ATCC TIB-152), J76 cells, and Ramos cells (ATCC CRL-1596) were cultured in RPMI-1640 (ATCC) supplemented with 10% FBS and penicillin-streptomycin. J76 cells were a gift from M. Heemskerk, Leiden University Medical Center, The Nederlands, and M. Davis, Stanford University, Stanford, CA). TCR- and BCR-expressing cell lines were generated as previously described (15). ACE2-expressing cells were generated by lentiviral transduction of Jurkat cells with lentivirus produced with a pHIV-hACE2-EGFR followed by cell sorting.

**Plasmid Construction.** Peptides displayed by HLA-A*02:01 were encoded as single-chain trimers in pHIV transfer plasmids as previously described (15). The complete native SARS-CoV-2 S sequence and complete prefusion-stabilized SARS-CoV-2 S (18) were synthesized as gBlocks (IDT) and cloned into the pMD2 plasmid backbone. CR3022 and VRC01 plasmids were generated as previously described (15).

**Lentiviral Vector Production and Purification.** HEK293T cells were transiently transfected with linear 25 kDa polyethylenimine (PEI; Santa Cruz Biotechnology) at a 3:1 mass ratio of PEI to DNA. DNA and PEI were diluted in Opti-MEM (Thermo Fisher), mixed, and incubated at room temperature for 15 min. The mixture was then added dropwise to 70 to 80% confluent HEK293T cells. After 3 to 6 h, media was changed to DMEM-HEPES (25 mM HEPES). The plasmid mass ratio of transfer plasmid to psPAX2.1 to pMD2 envelope plasmid (if used) to VSVGmut or VSVwt was 5.6:3:3:1 as previously described (15). SARS-CoV-2 S viruses were generated with pMD2-S (envelope), pHIV-GFP (transfer), psPAX2.1, and VSVG-mut. For a T225 flask and four plasmids, a total of 94.5 µg of DNA was used. If an envelope plasmid was not required, 72 µg of DNA was used.

After 48 h, unconcentrated virus was collected, centrifuged for 5 min at 300 g to pellet debris, filtered (0.45 µm polyethersulfone), and concentrated by ultracentrifugation for 90 min at 100,000 g at 4 °C. The supernatant was removed and viral pellets were resuspended in Opti-MEM overnight at 4 °C. Concentrated virus was aliquoted and stored at -80C until use. Prior to use, virus was thawed at 4 °C.

**Cell Line Transduction Assay.** Single concentrated lentivirus and cells (Ramos, J76, or Jurkat) were mixed in the indicated amounts with 8 μg/mL diethylaminoethyl-dextran (Sigma-Aldrich). After 24 h, an additional 0.5× of media was added. Cells were analyzed by flow cytometry on a Cytoflex S after 48 h.

**Primary Cell Activation, Proliferation, and Transduction Assay.** Deidentified peripheral blood mononuclear cells from healthy donors were obtained from leukopaks purchased from Stem Cell Technologies. Cells were purified using Ficoll-Paque PLUS (GE Healthcare) density gradient centrifugation with SepMate tubes (Stem Cell Technologies) according to the manufacturer's instructions. Primary $CD8^+$ T cells were isolated using EasySep Human $CD8^+$ T Cell Enrichment kits (Stem Cell Technologies) and cultured in RPMI-1640 (ATCC) supplemented with 10% FBS, penicillin-streptomycin, and 50 IU/mL recombinant human IL-2 (R&D Systems). Following isolation, cells were immediately stained with CellTrace dye (Thermo Fisher) according to the manufacturer's instructions (day 0). The T cells were rested overnight at 37C/5% $CO_2$. On day 1, cells were treated with either concentrated lentivirus or DynaBeads Human T-Activator CD3/CD28 (Thermo Fisher) at a 1:1 cell-to-bead ratio. For lentivirus, a dose series of concentrated lentivirus was prepared and cells were added with 8 μg/mL diethylaminoethyl-dextran (Sigma-Aldrich). Concentrated lentiviruses displaying CoV-2 S, prefusion-stabilized S-2P CoV-2 S, anti-CD3-CD80, and HLA-A2-NYESO were added. After 24 h (day 2), cells were sampled to assess activation with anti-CD69 and anti-CD25 antibodies (BioLegend) on a Cytoflex S flow cytometer. Cells were additionally stained with V-region antibodies for TRBV5-6 (Vbeta5.2, Beckman Coulter), TRBV14 (Vbeta16, Miltenyi Biotec), and TRBV13 (Vbeta23, Miltenyi Biotec). On day 10, cells were analyzed for transduction (GFP expression) and proliferation (CellTrace dye dilution) via flow cytometry. Cells were stained with LIVE/DEAD fixable viability dye according to the manufacturer's instructions on both days 2 and 10.

**Flow Cytometry.** Antibodies were used at the following dilutions from stock concentrations: anti-CD69 (1:200), anti-CD25 (1:200), anti-TRBV5-6 (1:50), anti-TRBV14 (1:200), and anti-TRBV13 (1:100). All flow analysis was completed using a Cytoflex S flow cytometer. Unless otherwise noted, cells were stained with antibodies for 20 min in FACS buffer (PBS + 0.1% BSA and 1 mM EDTA) followed by two washes with FACS buffer prior to analysis via flow cytometry.

**Recombinant Protein Production.** Variants of the $gp100_{209}$ peptide were commercially synthesized at >80% purity (Genscript); variants used were the previously studied position 2 methionine ($gp100_{209\text{-}2M}$) and position 2 norleucine ($gp100_{209\text{-}2Nle}$) peptides (14). Recombinant T4H2 TCR and the peptide/HLA-A*02:01 complexes were purified as previously described (14) Briefly, TCR α- and β-chains, the HLA-A*02:01 heavy chain, and $\beta_2$-microglobulin ($\beta_2$m) were expressed as inclusion bodies in *Escherichia coli* and were dissolved in 6 M guanidine, 10 mM sodium acetate, 10 mM EDTA, pH 4.2 following purification. For refolding, TCR α and β chains were rapidly diluted into 50 mM Tris·HCl (pH 8.3), 2.5 M urea, 6.3 mM cysteamine, 3.7 mM cystamine, 2 mM EDTA, and 0.2 mM PMSF. HLA-A*02:01 heavy chain and $\beta_2$m in a 1:1 molar ratio were rapidly diluted into 100 mM Tris·HCl (pH 8.3), 400 mM L-arginine, 6.3 mM cysteamine, 3.7 mM cystamine, 2 mM EDTA, and 0.2 mM PMSF with 30 mg/mL peptide. TCR and peptide/MHC were incubated in refold buffers for 12 h at 4 °C followed by dialysis against 10 mM Tris·HCl (pH 8.3) for 48 h. The TCR and peptide/HLA-A*02:01 complexes were purified by anion exchange followed by size-exclusion chromatography. Recombinant SARS-CoV S (catalog no. 10683-CV, lot no. DOXT0121071) and human ACE-2 (catalog no. 933-ZN, lot no. FIU620051) were obtained lyophilized from R&D systems and reconstituted in phosphate-buffered saline per the manufacturer's instructions. Prior to use samples were buffer exchanged into 10 mM HEPES (pH 7.4), 150 mM NaCl, 3 mM EDTA, and 0.005% surfactant P-20 (HBS-EP) and used without further purification.

**SPR.** SPR experiments were performed using a Biacore T200 instrument (GE Healthcare). All proteins were buffer exchanged into HBS-EP running buffer prior to measurements; the TCR was exchanged chromatographically; due to limited sample, ACE-2 was exchanged using microcentrifugal filters with a 10,000 kD molecular weight cutoff. S protein and peptide/HLA-A*02:01 were immobilized on a CM5 Series S sensor chip (Cytiva) via amine coupling to RUs of approximately 300 for S protein and 3,000 to 4,000 for peptide/HLA-A*02:01. Increasing concentrations of TCR were injected as indicated at a flow rate of 5 μL/min. ACE-2 was injected at a concentration of 10 nM at a flow rate of 5 μL/min after TCR injections. Experiments were performed at 25 °C with a blank activated/deactivated flow cell as a reference. All injections were repeated twice and are shown as blank-subtracted responses. The binding affinity between the TCR and peptide/HLA-A*02:01 was determined by fitting reference corrected steady-state values (taken approximately 5 s prior to the end of the injection) to a single site binding isotherm. Both datasets were fit simultaneously; reported error is the SE from the fit. Despite multiple centrifugal buffer exchanges, the ACE-2 sample retained a mismatch with the HPS-EP running buffer, resulting in an additional bulk refractive index shift after injection. This was determined from the negative deflection after the immediate start of association phase, and for Fig. 1*D*, the resulting correction of 345 RU was applied to the pre- and postinjection signals, leaving the reference-corrected binding response unaltered. The SPR data in Fig. 1 are one of two replicates with the same overall outcome, except the replicate for TCR binding to peptide/HLA-A*02:01 used the $gp100_{209\text{-}2Nle}$ peptide, yielding a $K_D$ of 8 ± 2 μm.

**Statistical Analysis.** Graphs and statistical analyses were generated using GraphPad Prism (version 9) and OriginPro 2024. Data are shown as mean ± SD as indicated in figure legends, except where indicated. Statistical tests are described in figure legends. $P$ values $< 0.05$ were considered statistically significant and are reported in figures and figure legends. Data fitting for the T4H2 TCR $K_D$ was performed with OriginPro 2024. Flow cytometry data were analyzed with FlowJo (version 10.8.1).

**Data, Materials, and Software Availability.** All study data are included in the article and/or *SI Appendix*.

**ACKNOWLEDGMENTS.** We thank Blake Smith for his technical assistance. This work was supported by a Canadian Institutes of Health Research Doctoral Foreign Study Award to S.A.G. and by the NIH (DP2AI158126 to M.E.B. and R35GM118166 to B.M.B.). This work was supported in part by the Koch Institute Support (core) Grant 5P30-CA014051 from the National Cancer Institute. We thank the Koch Institute's Robert A. Swanson (1969) Biotechnology Center for technical support with flow cytometry.

Author affiliations: [a]Department of Chemical Engineering, Massachusetts Institute of Technology, Cambridge, MA 02139; [b]Koch Institute for Integrative Cancer Research, Massachusetts Institute of Technology, Cambridge, MA 02139; [c]Department of Chemistry and Biochemistry, University of Notre Dame, South Bend, IN 46556; [d]Harper Cancer Research Institute, University of Notre Dame, South Bend, IN 46556; [e]Department of Biological Engineering, Massachusetts Institute of Technology, Cambridge, MA 02139; and [f]Ragon Institute of Massachusetts General Hospital, Massachusetts Institute of Technology, and Harvard, Cambridge, MA 02139

Author contributions: S.A.G., B.M.B., and M.E.B. designed research; S.A.G., T.J.R., and L.S.-H. performed research; S.A.G., T.J.R., and L.S.-H. analyzed data; and S.A.G., B.M.B., and M.E.B. wrote the paper.

1. J. Shang *et al.*, Cell entry mechanisms of SARS-CoV-2. *Proc. Natl. Acad. Sci. U.S.A.* **117**, 11727–11734 (2020).
2. M. H. Cheng *et al.*, Superantigenic character of an insert unique to SARS-CoV-2 spike supported by skewed TCR repertoire in patients with hyperinflammation. *Proc. Natl. Acad. Sci. U.S.A.* **117**, 25254–25262 (2020).
3. M. Noval Rivas, R. A. Porritt, M. H. Cheng, I. Bahar, M. Arditi, Multisystem inflammatory syndrome in children and long COVID: The SARS-CoV-2 viral superantigen hypothesis. *Front. Immunol.* **13**, 941009 (2022).
4. M. H. Cheng *et al.*, A monoclonal antibody against staphylococcal enterotoxin B superantigen inhibits SARS-CoV-2 entry in vitro. *Structure* **29**, 951–962.e3 (2021).
5. R. A. Porritt *et al.*, HLA class I-associated expansion of TRBV11-2 T cells in multisystem inflammatory syndrome in children. *J. Clin. Invest.* **131**, e146614 (2021).
6. Z. Zhang *et al.*, Enhanced CD95 and interleukin 18 signalling accompany T cell receptor Vβ21.3+ activation in multi-inflammatory syndrome in children. *Nat. Commun.* **15**, 1–16 (2024).
7. P. Brodin, M. Arditi, Severe acute hepatitis in children: Investigate SARS-CoV-2 superantigens. *Lancet Gastroenterol. Hepatol.* **7**, 594–595 (2022).
8. A. M. Deacy, S. K.-E. Gan, J. P. Derrick, Superantigen recognition and interactions: Functions, mechanisms and applications. *Front. Immunol.* **12**, 731845 (2021).
9. M. M. Karunakaran *et al.*, Butyrophilin-2A1 directly binds germline-encoded regions of the Vγ9Vδ2 TCR and is essential for phosphoantigen sensing. *Immunity* **52**, 487–498.e6 (2020).
10. J. Lu *et al.*, Structure of MHC-independent TCRs and their recognition of native antigen CD155. *J. Immunol.* **204**, 3351–3359 (2020).

11. A. N. Tikhonova *et al.*, $A\beta$ T cell receptors that do not undergo major histocompatibility complex-specific thymic selection possess antibody-like recognition specificities. *Immunity* **36**, 79–91 (2012).
12. R. T. Kubo, W. Born, J. W. Kappler, P. Marrack, M. Pigeon, Characterization of a monoclonal antibody which detects all murine alpha beta T cell receptors. *J. Immunol.* **142**, 2736–2742 (1989).
13. C. Amormino *et al.*, SARS-CoV-2 spike does not possess intrinsic superantigen-like inflammatory activity. *Cells* **11**, 2526 (2022).
14. A. R. Smith *et al.*, Structurally silent peptide anchor modifications allosterically modulate T cell recognition in a receptor-dependent manner. *Proc. Natl. Acad. Sci. U.S.A.* **118**, e2018125118 (2021).
15. C. S. Dobson *et al.*, Antigen identification and high-throughput interaction mapping by reprogramming viral entry. *Nat. Methods* **19**, 449–460 (2022).
16. G. B. E. Stewart-Jones, A. J. McMichael, J. I. Bell, D. I. Stuart, E. Y. Jones, A structural basis for immunodominant human T cell receptor recognition. *Nat. Immunol.* **4**, 657–663 (2003).
17. M. Yuan *et al.*, A highly conserved cryptic epitope in the receptor binding domains of SARS-CoV-2 and SARS-CoV. *Science* **368**, 630–633 (2020).
18. D. Wrapp *et al.*, Cryo-EM structure of the 2019-nCoV spike in the prefusion conformation. *Science* **367**, 1260–1263 (2020).
19. M. Baek *et al.*, Accurate prediction of protein structures and interactions using a three-track neural network. *Science* **373**, 871–876 (2021).
20. J. Abramson *et al.*, Accurate structure prediction of biomolecular interactions with AlphaFold 3. *Nature* **630**, 493–500 (2024).
21. M. F. Lensink *et al.*, Prediction of protein assemblies, the next frontier: The CASP14-CAPRI experiment. *Proteins* **89**, 1800–1823 (2021).
22. D. Wu *et al.*, Structural characterization and AlphaFold modeling of human T cell receptor recognition of NRAS cancer neoantigens. bioRxiv [Preprint] (2024). https://doi.org/10.1101/2024.05.21.595215 (Accessed 6 July 2024).
23. P. Bradley, Structure-based prediction of T cell receptor:Peptide-MHC interactions. *Elife* **12**, e82813 (2023).